Inorganic Chemistry

Article

pubs.acs.org/IC

Effect of Synthetic Levers on Nickel Phosphide Nanoparticle Formation: Ni_5P_4 and NiP_2

Da Li, Keerthi Senevirathne,[†] Lance Aquilina, and Stephanie L. Brock*

Department of Chemistry, Wayne State University, Detroit, Michigan 48202, United States

Supporting Information

ABSTRACT: Due to their unique catalytic, electronic, and redox processes, Ni_5P_4 and NiP_2 nanoparticles are of interest for a wide-range of applications from the hydrogen evolution reaction to energy storage (batteries); yet synthetic approaches to these materials are limited. In the present work, a phase-control strategy enabling the arrested-precipitation synthesis of nanoparticles of Ni_5P_4 and NiP_2 as phase-pure samples using different Ni organometallic precursors and trioctylphosphine (TOP) is described. The composition and purity of the product can be tuned by changing key synthetic levers, including the Ni precursor, the oleylamine (OAm) coordinating solvent and TOP concentrations, temperature, time, and the presence or absence of a moderate temperature soak step to facilitate formation of Ni and/or Ni−P amorphous nanoparticle intermediates. Notably, the 230 °C intermediate step favors the ultimate formation of Ni_2P and hinders further phosphidation to form Ni_5P_4 or NiP_2 as phase-pure products. In the absence of this step, increasing the P/Ni ratio (13−20), reaction temperature (350−385 °C), and time (10−48 h) favors more P-rich phases, and these parameters can be adjusted to generate either Ni_5P_4 or NiP_2. The phase of the obtained particles can also be tuned between pure Ni_2P to Ni_5P_4 and NiP_2 by simply decreasing the OAm/TOP ratio and/or changing the nickel precursor (nickel(II)acetylacetonate, nickel(II)acetate tetrahydrate, or bis(cyclooctadiene)nickel(0)). However, at high concentrations of OAm, the product formed is the same regardless of Ni precursor, suggesting the formation of a uniform Ni intermediate (an Ni-oleylamine complex) under these conditions that is responsible for product distribution. Intriguingly, under the extreme phosphidation conditions required to favor Ni_5P_4 and NiP_2 over Ni_2P (large excess of TOP), the 20−30 nm crystallites assemble into supraparticles with diameters of 100−500 nm. These factors are discussed in light of a comprehensive synthetic scheme utilized to control P incorporation in nickel phosphides.

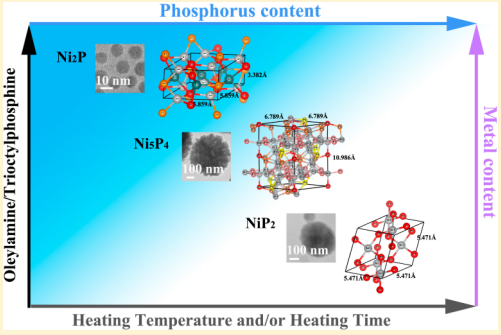

INTRODUCTION

Due to the wide range of unique magnetic, redox, and catalytic properties exhibited by transition metal phosphides, the development of methods for their production on the nanoscale with control of size, shape, and composition is an important endeavor.[1−4] Because the magnetic and catalytic properties of transition metal phosphides depend on the size and shape (in the nano regime) as well as the composition,[5−9] it is important to establish the synthetic factors that enable access to different phase-pure transition metal phosphides. Metal-rich nickel phosphides such as Ni_2P are potent hydrotreating catalysts[1,2,5,8,10−12] while the more phosphorus-rich phases such as Ni_5P_4 and NiP_2 are promising candidates for lithium ion battery electrode materials due to their high gravimetric and volumetric capacity.[13,14] Furthermore, all of these phases show considerable potential to be used in hydrogen evolution catalysis.[15−17]

Nanoparticles of metal-rich nickel phosphides can be synthesized by the decomposition of organometallic species, or decomplexation of metal complexes, to generate active nickel species, and their subsequent reaction with alkyl phosphines (e.g., trioctylphosphine TOP).[18] While the reactive form of P is not known, PH_3 generated from alkene elimination steps has been purported to be the active species in nickel phosphide formation. Thus, TOP acts as both a coordinating solvent and a reactant and is used as a nonstoichiometric precursor (in large excess), making it difficult to control the evolution between different phases. The Brock group first reported on the formation of solid spherical Ni_2P nanoparticles prepared by the reaction of bis(1,5-cyclooctadiene)-nickel(0) [$Ni(COD)_2$] and TOP at 345 °C in trioctylphosphine oxide (TOPO).[8] Another study by the Brock group, in which nickel acetylacetonate was used as the nickel source, established the role of reaction parameters, such as reactant concentration, time, temperature, and cosolvent (oleylamine), in determining the final stoichiometric phase, $Ni_{12}P_5$ vs Ni_2P, and the degree to which hollow particles formed due to the Kirkendall effect.[19] This study and others showed that precursor particles, which serve as templates for the final crystalline phosphide product, form when the reactants are first heated at 230 °C.[19] For P/Ni ratios larger than 2.24, heating the Ni source and TOP at 230 °C will form relatively small (<10 nm) amorphous Ni_xP_y nanoparticles, whereas at lower ratios, relatively large (>20 nm) crystalline Ni

Received: May 18, 2015
Published: August 4, 2015

DOI: 10.1021/acs.inorgchem.5b01125
Inorg. Chem. 2015, 54, 7968−7975

Scheme 1. Synthesis of Nickel Phosphide Nanoparticles

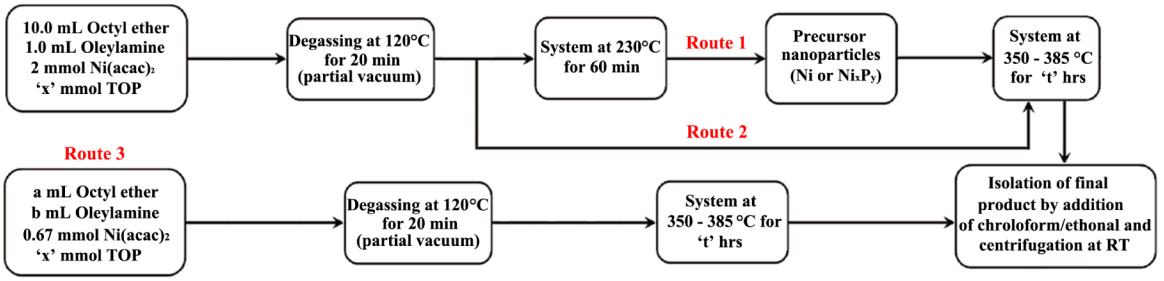

nanoparticles are formed as the templating intermediates. Increasing TOP quantity, reaction temperature, and reaction time favors the transformation of the intermediate particles to the Ni_2P phase in lieu of the more metal-rich $Ni_{12}P_5$ phase. In contrast, increasing the oleylamine (OAm), which served as both a reducing agent and surfactant, relative to nickel results in a more metal-rich phase and reduces the Kirkendall effect, resulting in a reduction in the size of hollows in particles prepared from large crystalline Ni nanoparticle templates.[19]

Despite considerable attention on metal-rich phosphides, little research on the synthesis of phosphorus-rich nickel phosphide nanoparticles has been published.[14,20] The Tatsumisago group reported a synthetic method for phase-pure Ni_5P_4 and NiP_2, with the phase selectivity achieved by using different Ni precursors (nickel acetylacetonate and nickel acetate tetrahydrate) in combination with TOP in TOPO, but the mechanism of phase control and the key factors that underscore selectivity were not presented.[14] In order to be able to target desired phases on the more phosphorus-rich side of the Ni−P phase diagram, a detailed study of the parameters that govern phase formation is needed.

Our objectives are to (1) extend the successful phase control strategy used for nickel-rich $Ni_{12}P_5$−Ni_2P to the more phosphorus-rich phases, Ni_5P_4−NiP_2; (2) study the role of the key synthetic levers on the phase-purity and morphology of the product, including the Ni precursor, the OAm and TOP concentrations, temperature, time, and the explicit formation of Ni/amorphous Ni−P intermediate nanoparticles by a moderate temperature soak step; and (3) develop a comprehensive synthetic scheme to control phosphorus incorporation in nickel phosphides prepared by arrested precipitation reaction.

EXPERIMENTAL SECTION

Materials. Nickel acetylacetonate ($Ni(acac)_2$, 95%) and bis(1,5-cyclooctadiene)nickel(0) ($Ni(COD)_2$, 98%) were purchased from Alfa Aesar. Nickel(II) acetate tetrahydrate ($Ni(OAc)_2{\cdot}4H_2O$, 99%) was purchased from Sigma-Aldrich. Tri-*n*-octylphosphine (TOP, 97%) was purchased from STREM. *n*-Octyl ether (OE) was purchased from TCI America. Oleylamine (OAm, C18 content 80−90%) was purchased from ACROS. Chloroform and ethanol (200 proof) were purchased from Fisher Scientific and Decon Laboratories, Inc., respectively. All chemicals were used as received.

Synthesis. ***Safety warning!*** *This procedure involves the use of organometallic and organic reagents at elevated temperatures and should be conducted under an inert atmosphere to avoid a potentially explosive reaction with air. Toxic and flammable PH_3 gas is potentially produced as an intermediate; therefore the reaction should be conducted in a fume hood.* All reactions were carried out in the fume hood under an argon atmosphere using standard Schlenk line techniques and following the procedure outlined in Scheme 1. The flasks were heated in mantles insulated with quartz wool, and the temperature was monitored using a probe adjacent to the flask, and within the mantle.

Routes 1 and 2. The synthesis of Ni/Ni_xP_y precursor particles was performed by taking 0.514 g of $Ni(acac)_2$ (2.0 mmol), 12.0−30.0 mL (26.9−67.2 mmol) of TOP, 10.0 mL of octyl ether, and 1.0 mL of OAm (3.0 mmol) and heating at 230 °C for 60 min. The system temperature was then raised to 350−385 °C, kept for 1−24 h, and then allowed to cool naturally to room temperature. In route 2, the intermediate 230 °C step was removed. When $Ni(COD)_2$ or $Ni(OAc)_2.4H_2O$ was used as a metal precursor, all the reaction parameters were identical except that 0.550 g of $Ni(COD)_2$ (2.0 mmol) or 0.498 g of $Ni(OAc)_2{\cdot}4H_2O$ (2.0 mmol) was employed in lieu of $Ni(acac)_2$.

Route 3. A mixture of 0.172 g of $Ni(acac)_2$ (0.67 mmol), 1−20 mL of TOP (2.2−44.8 mmol), and 10 mL of a mixture of OAm and octyl ether ranging from 3.3% up to 100% OAm (1.0−30.0 mmol) by volume was directly heated at 330−385 °C for 1−48 h and then allowed to cool naturally to room temperature. The reaction was conducted similarly for $Ni(COD)_2$ or $Ni(OAc)_2{\cdot}4H_2O$, using 0.183 g of $Ni(COD)_2$ (0.67 mmol) or 0.166 g of $Ni(OAc)_2{\cdot}4H_2O$ (0.67 mmol).

The black precipitates from routes 1−3 (nickel phosphide nanoparticles) were sonicated in chloroform and reprecipated by adding excess ethanol. This sonication-precipitation cycle was done at least three times to remove as much of the bound organics as possible from the system. The isolated black powder was then dried under a vacuum.

Characterization Techniques. Powder X-ray diffraction (PXRD) was carried out on a Bruker D2 Phaser X-ray diffractometer using the Kα line of a Cu source. Samples were deposited onto a zero background quartz holder, and data were acquired in the 2θ range 20−60° with a step size of 0.02°. PXRD patterns were processed using Jade 5.0 software and compared to powder diffraction files (PDFs) from the ICDD database.

Electron microscopy and energy dispersive spectroscopy (EDS) were performed using a JEOL 2010 electron microscope operated at a voltage of 200 kV and a beam current of 107−108 μA with a coupled EDS detector (EDAX Inc.). The images were captured using Amtv600 software provided by the Advanced Microscopy Techniques Corporation. Samples for TEM analysis were prepared by depositing a drop of a chloroform nanoparticle dispersion onto a carbon-coated 200 mesh Cu grid, followed by air-drying.

RESULTS AND DISCUSSION

At the outset, $Ni(acac)_2$ was used as the metal source and TOP as the P source to prepare nickel phosphide nanoparticles. Our previous work on nanoscale iron phosphides clearly indicated that the choice of P/M (phosphorus/metal) precursor ratio, reaction temperature, and heating time are key factors that determine the stoichiometry of the product.[6] A series of reactions were carried out following route 1 (Scheme 1) to establish the independent effects of TOP/Ni ratio, heating temperature, and reaction time. Relative to our prior work on $Ni_{12}P_5$ and Ni_2P, we sought to use higher P/M ratios, temperatures, and times in order to achieve increased phosphidation.

DOI: 10.1021/acs.inorgchem.5b01125
Inorg. Chem. 2015, 54, 7968−7975

Effect of Precursor Ratio, Temperature, and Time: Route 1. Using a synthesis temperature of 370 °C and 3 mmol OAm, the ratio of P/Ni in the reaction was varied from 13.4 to 20.2 by changing the quantity of TOP (26.8 to 40.4 mmol) used in the synthesis. As shown in Figure 1, when the P/Ni ratio was changed from 13.4 to 16.8, the phase of the final product changed from Ni_2P to a mixture of Ni_2P and Ni_5P_4. Further increasing the P/Ni ratio to 18.8 resulted in a mixture of Ni_2P, Ni_5P_4, and NiP_2, whereas for a P/Ni ratio of 20.2, NiP_2 was the major phase (with Ni_2P, NiP, and Ni_5P_4 present as minor phases). These data suggest that higher concentration of TOP favors the incorporation of more P into the nickel phosphide nanoparticles.

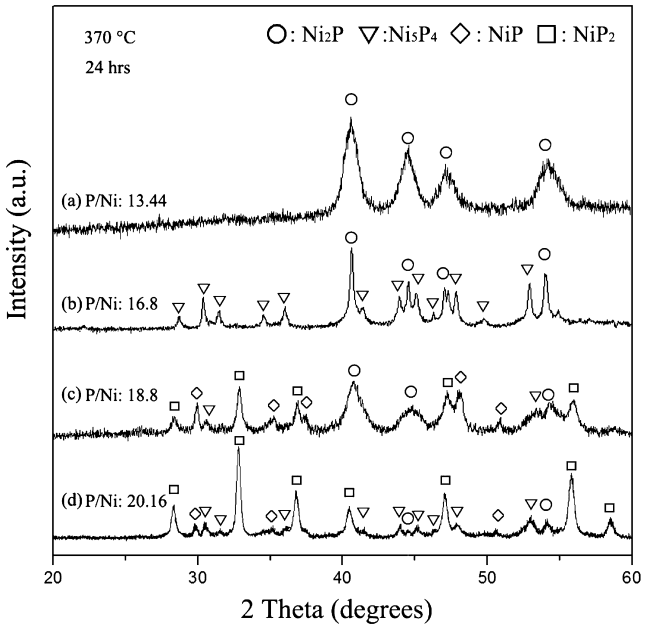

Figure 1. PXRD patterns of the product from route 1 (Scheme 1) as a function of TOP quantity. Reactions were carried out at 370 °C for 24 h with 2 mmol $Ni(acac)_2$ and 3 mmol OAm.

In order to assess how temperature affects the final phase, the intermediate P/Ni ratio (16.8) was chosen, and the heating temperature was changed from 350 to 370 to 385 °C. As shown in Figure 2a, increasing temperature resulted in a shift in the product phase from Ni_2P (350 °C) to a mixture of Ni_2P and Ni_5P_4 (370 °C), and ultimately to a mixture of Ni_2P, Ni_5P_4, and NiP_2 (385°). Thus, the increase of heating temperature correlates with the appearance of more P-rich phases, presumably, by increasing the concentration of active phosphorus as well as the kinetics of P incorporation.

Finally, in order to assess how reaction time affects the final phase, the reaction time was varied from 10 to 24 to 48 h, holding the P/Ni ratio and heating temperature constant (16.8 and 370 °C, respectively). As shown in Figure 2b, the phase of the products changed from Ni_2P at 10 h to a mixture of Ni_2P and Ni_5P_4 at 24 h, and a mixture of Ni_2P, Ni_5P_4, NiP, and NiP_2 at 48 h demonstrating that longer reaction times also facilitate P incorporation.

The results clearly indicate that the higher P/Ni ratio, higher temperature, and the longer heating time favor the formation of P-rich phases. These observations are consistent with the behavior exhibited in the $Ni_{12}P_5$–Ni_2P case in our previous study, although in the present case the quantity of TOP used in the synthesis is much higher.[19] However, despite a clear preference toward more P-rich phases, it was impossible to obtain phase-pure products of Ni_5P_4 or NiP_2 by this approach. We hypothesized that Ni_2P, once formed, may be slow to convert and focused our study on the intermediate heating step.

Probing the Intermediate Heating Step. Previous studies showed that $Ni(acac)_2$ can be reduced by OAm ($0.1 \leq Ni/OAm \leq 0.33$) to Ni nanoparticles (without TOP or with low TOP/Ni ratio ($P/Ni < 2.24$)) or amorphous Ni_xP_y nanoparticles ($P/Ni > 2.24$) at 220–240 °C.[19,21,22] These nanoparticles then serve as templates for the formation of crystalline nickel phosphide nanoparticles at elevated temperatures.[19,23−25] As shown in Figure 3, we find that intermediate amorphous Ni_xP_y particles form in as little as 3 min at 230 °C (ca. 5.1 ± 0.6 nm, Figure 3), which means that whether or not there is an intermediate 230 °C step, this fast amorphous particle formation process may always occur during temperature ramp-up. At 60 min, the material remains amorphous, but the average particle size increases to 9.7 ± 1.6 nm. Intriguingly, heating for 24 h yields crystalline Ni_2P with a crystallite size diameter of 8.5 nm (calculated by applying the Scherrer equation to the (111) reflection), superimposed over an amorphous hump. This suggests that Ni_2P may be kinetically favored at lower T (230 °C), regardless of P/Ni ratio, and

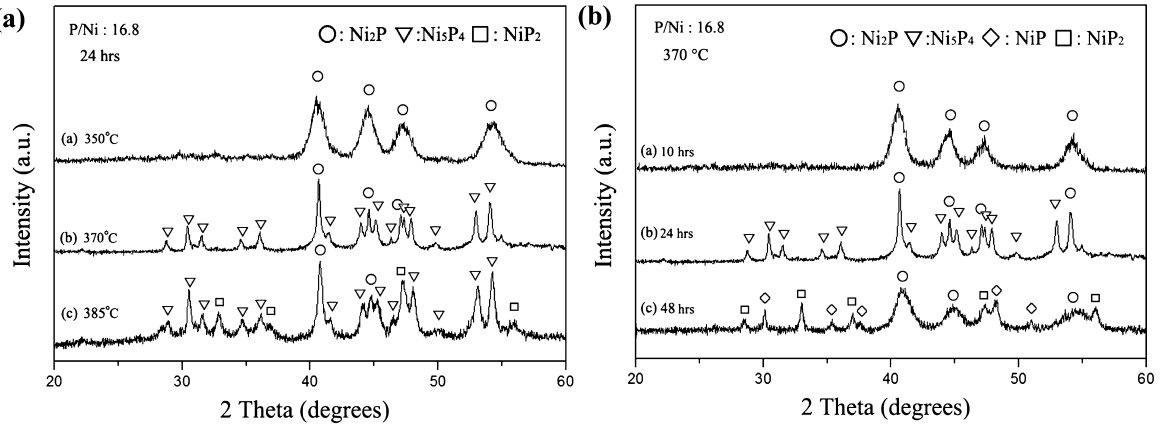

Figure 2. PXRD patterns of the products from route 1 (Scheme 1) with 2 mmol $Ni(acac)_2$ and 33.6 mmol TOP (P/Ni = 16.8). (a) As a function of heating temperature for 24 h; (b) as a function of heating time at 370 °C.

DOI: 10.1021/acs.inorgchem.5b01125
Inorg. Chem. 2015, 54, 7968−7975

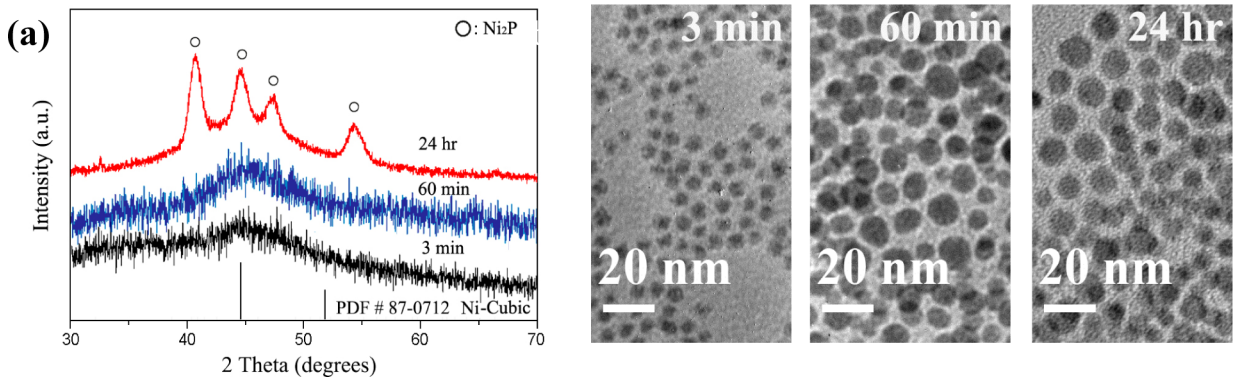

Figure 3. (a) PXRD patterns and (b) TEM images of intermediate Ni_xP_y particles prepared at different heating times at 230 °C (P/Ni = 16.8).

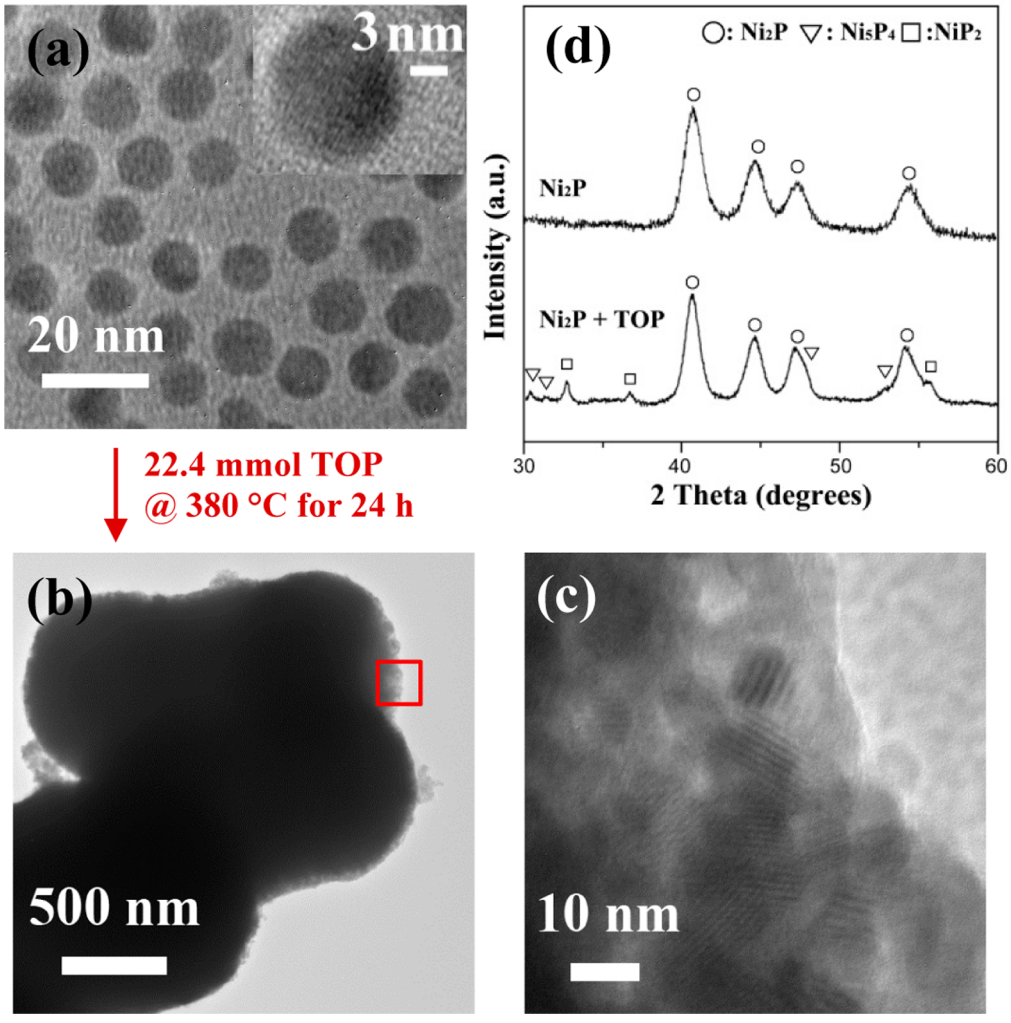

Figure 4. TEM images of Ni_2P nanoparticles (a) before and (b) after reaction with TOP. (c) HRTEM of a selected area in b. (d) PXRD patterns of Ni_2P particles before (top) and after (bottom) reaction with TOP at 380 °C for 24 h.

might be resistant to transformation to more P-rich phases, resulting in mixed phase products.

To test this premise, 0.5 mmol of Ni_2P nanoparticles (74.2 mg, 10 nm, Figure 4a) were synthesized and reacted with a large excess of TOP (22.4 mmol) in 10 mL of octyl ether at a high temperature (380 °C) for a long reaction time (24 h). Ni_2P was still the major phase observed in the final product along with some peaks attributed to Ni_5P_4 and NiP_2 determined by PXRD data (Figure 4d bottom). This is consistent with former work done by the Sanchez group showing that Ni_2P is a favored phase on the nanoscale even at high P/Ni ratios.[23] The formation of Ni_2P in the intermediate step and the inaccessibility of the complete conversion from Ni_2P to the more P-rich nickel phosphides suggest that increasing the duration of the intermediate step may facilitate crystallization of the amorphous particles, resulting in stabilizing the formation of Ni_2P and hindering further phosphidation to achieve the more P-rich phases as single-

DOI: 10.1021/acs.inorgchem.5b01125
Inorg. Chem. 2015, 54, 7968−7975

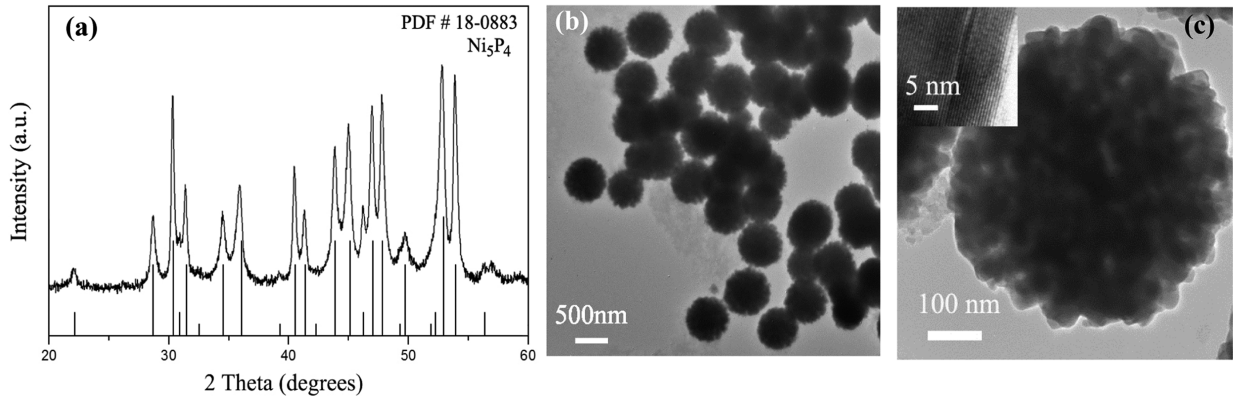

Figure 5. (a) PXRD pattern of Ni_5P_4 particles from route 2. (b, c) TEM images of Ni_5P_4 particles (inset: HRTEM showing lattice fringes).

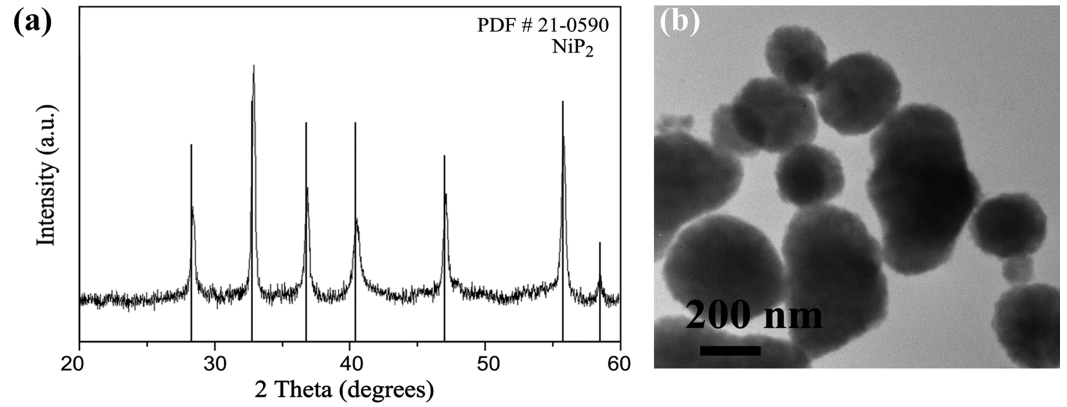

Figure 6. (a) PXRD patterns and (b) TEM images of NiP_2 particles prepared from route 2.

phase products. The consequences of the extreme phosphidation conditions on the morphology are shown in Figure 4b, where the products are spherical clusters of 500 nm in diameter. High resolution TEM imaging of a selected area (Figure 4c) reveals that these clusters comprise a large amount of well-crystallized 10 nm Ni_2P nanoparticles. As will be shown below, the combination of high TOP amount and high temperature favors large aggregates of discrete nanoparticles, reminiscent of supraparticles.[26] Based on the fact that the primary particles remain small and of an appropriate size to undergo further phosphidation, we attribute the minimal conversion to the stability of Ni_2P.

Obtaining Phase-pure Ni_5P_4 by Route 2. In order to avoid Ni_2P formation at the intermediate step, the 230 °C step was eliminated as shown in route 2 (Scheme 1). For a P/Ni ratio of 16.8, raising the reaction temperature directly to 370 °C for 24 h leads to a material wherein the detectable PXRD peaks could all be indexed to Ni_5P_4 (Figure 5a). Crystallite size calculated by applying the Scherrer equation to the (214) reflection of Ni_5P_4 nanoparticles yielded an average diameter of 25.3 nm. Transmission electron microscopy (TEM) images (Figure 5b and c) reveal that the Ni_5P_4 product forms as highly uniform spherical supraparticles of ca. 500 nm in diameter consisting of many small 20−30 nm nanocrystallites, similar to what was observed from forced phosphidation of Ni_2P. This phenomenon has also been observed in other systems with quite different chemistries, including Fe_3O_4, In_2O_3, and CdSe.[27−29] The primary particles are presumed to aggregate into supraparticles in order to minimize the surface energy.

Obtaining Phase-pure NiP_2 by Route 2. In order to target a more P-rich phase (NiP or NiP_2), the P/Ni ratio and heating temperature were increased from 16.8 to 33.6 and 370 to 385 °C, respectively, in route 2 (without the 230 °C step). PXRD data acquired on the product are consistent with the formation of NiP_2 (Figure 6). From the Scherrer equation, the crystallite size of these NiP_2 particles is about 29.6 nm, whereas the particle size obtained from TEM micrographs is quite large (hundreds of nanometers), suggesting that particle aggregation and supraparticle formation is again operable. Intriguingly, these particles are less uniform than those obtained at 370 °C, suggesting that the formation of discrete NiP_2 particles and aggregation into supraparticles may not be temporally isolated in this case.

Obtaining Pure-phase Ni_2P by Route 2. We next tested whether the intermediate templating step was needed for routine Ni_2P particle formation and whether it has any role in dictating particle size or polydispersity. We synthesized Ni_2P nanoparticles according to both route 1 and route 2 with identical reagent parameters, except one had the intermediate step and the other did not. There is no obvious difference between the crystallite size from PXRD or the size/morphology from TEM of the phase-pure Ni_2P nanoparticles prepared by these two routes (Figure S1). Therefore, for nanoscale nickel phosphide formation, the introduction of an explicit moderate temperature soak step to form intermediate precursor particles that template formation of the product is not necessary.

Effect of the Nickel Precursor on Targeted Phase. Based on the prior work showing the Ni precursor can affect the targeted phases, $Ni(acac)_2$, $Ni(COD)_2$, and $Ni(OAc)_2$·

DOI: 10.1021/acs.inorgchem.5b01125
Inorg. Chem. 2015, 54, 7968−7975

$4H_2O$ were used as Ni precursors in route 2 targeting conditions for Ni_5P_4 formation (P/Ni ratio = 16.8, 370 °C, 24 h). As evidenced from PXRD, the final phases of the products were Ni_5P_4 ($Ni(acac)_2$) and a mixture of Ni_5P_4, Ni_2P ($Ni(COD)_2$), and Ni_2P ($Ni(OAc)_2{\cdot}4H_2O$) (Figure 7). We

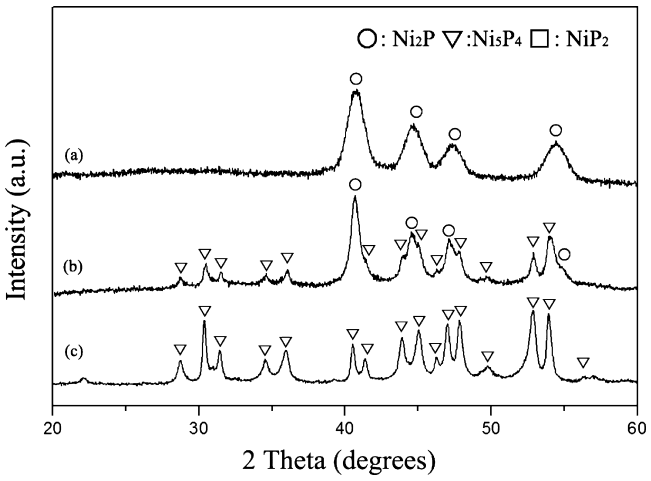

Figure 7. PXRD patterns of the product from route 2 (Scheme 1) using different Ni precursors: (a) $Ni(OAc)_2{\cdot}4H_2O$, (b) $Ni(COD)_2$, and (c) $Ni(acac)_2$.

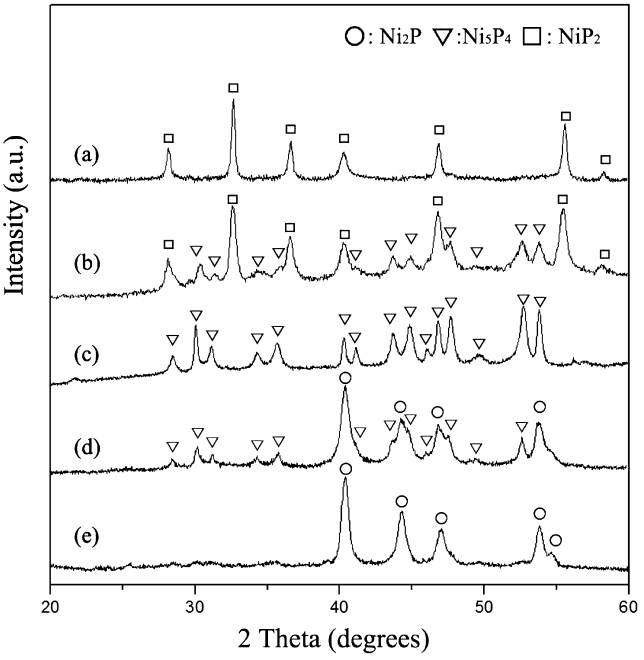

Figure 8. PXRD patterns of the products from route 3 (Scheme 1) as a function of OAm/TOP ratio. Reactions were carried out at 370 °C for 24 h with 0.73 mmol $Ni(acac)_2$.

hypothesized that the precursor dependence may be due to the different Ni release rates, which will in turn affect the available Ni concentration. For the case of $Ni(acac)_2$, the strong chelating effect will cause Ni to be reduced and released slowly, leading to a high P/Ni ratio in the early stages of the reaction relative to the weaker, coordinate bonded, $Ni(OAc)_2{\cdot}4H_2O$ case. Therefore, the final product favors the more P-rich phase Ni_5P_4 for $Ni(acac)_2$ whereas $Ni(OAc)_2{\cdot}4H_2O$ favors Ni_2P. For the organometallic precursor $Ni(COD)_2$, a combination of Ni_5P_4 and Ni_2P is produced, suggesting that this precursor is intermediate to $Ni(acac)_2$ and $Ni(OAc)_2{\cdot}4H_2O$ in its rate of Ni release. Intriguingly, our results are in direct contrast to those of the Tatsumisago group. In their study, when $Ni(OAc){\cdot}4H_2O$ was used as the precursor in the synthesis, the product favored the more P-rich product NiP_2 compared with Ni_2P produced by using $Ni(acac)_2$ as the precursor. One key difference between our work and that of the Tatsumisago group is the inclusion of OAm in our method; thus a series of reactions were done to further investigate the role the OAm plays in the synthesis.

Role of Oleylamine: Route 3. As mentioned above, in the absence of OAm, $Ni(OAc){\cdot}4H_2O$ is reported to favor the generation of NiP_2, whereas $Ni(acac)_2$ favors Ni_2P, in direct contrast to what we observe in our system with OAm. Accordingly, reactions with a varied OAm/TOP ratio were carried out in order to understand the effect of OAm on the synthesis (route 3, Scheme 1). Starting from conditions known to favor NiP_2, (i.e., a high TOP/Ni ratio (33.4) and low OAm/TOP ratio (0.045)), the amount of OAm was increased by replacing a portion of the octyl ether with OAm (decreasing a and increasing b, route 3), thus increasing the ratio of OAm/TOP. When OAm/TOP is increased from 0.045 to 0.67 and 1.34, the product phase changed from NiP_2 to a mixture of Ni_5P_4 and NiP_2, and then to Ni_5P_4 (Figure 8a,b,c). For the OAm/TOP ratio of 1.34, there was no octyl ether in the system; OAm was thus acting not only as a surfactant but also the sole solvent (a = 0, b = 10). Changing the reaction time from 1 to 48 h, the heating temperature from 350 to 385 °C, and the P/Ni ratio from 21.6 to 61.6 had no effect; the obtained phase in every case was Ni_5P_4 (Figure 8c, Supporting Information Figure S2).

We expect this observation reflects a balance between the high P/Ni ratio (>21.6) guaranteeing sufficient phosphidation of the final product to facilitate the formation of a P-rich phase, while at the same time, the high OAm/TOP ratio enables OAm to compete with TOP to bond with the particle surface, thereby limiting the quantity of TOP participating in the reaction. We considered whether the amine might react to promote PH_3 formation, but based on the fact that increasing OAm *decreases* the amount of phosphorus incorporated, it appears instead that it is the reducing nature of OAm that is contributing to the phase-stability balancing act. Thus, in pure OAm, the intermediate phosphided phase Ni_5P_4 is stable relative to NiP_2, even when the P/Ni ratio reaches as high as 61.6. In contrast, Ni_2P can be accessed by decreasing the TOP amount. Thus, when the OAm/TOP ratio was increased from 1.34 to 8.93 and to 13.4, the product phase changed from Ni_5P_4 to a mixture of Ni_5P_4 and Ni_2P, and subsequently, Ni_2P (Figure 8c,d,e). Accordingly, much lower P/Ni ratios are needed to favor Ni_2P in route 3 (high OAm/Ni; P/Ni = 3.34, Figure 7a), whereas in route 2, Ni_2P is favored even at relatively large P/Ni ratios (lower OAm/Ni; P/Ni = 13.44, Figure 1a). Intriguingly, under conditions where the OAm amount is high (a = 0, b = 10) in route 3, varying the Ni precursor ($Ni(acac)_2$, $Ni(COD)_2$, and $Ni(OAc)_2{\cdot}4H_2O$) has no effect on the outcome (Ni_5P_4), indicating that dissolving the different Ni sources in OAm may form a single precursor "Ni(OAm)," which favors the formation of Ni_5P_4 (unless the TOP concentration is dramatically reduced).

DOI: 10.1021/acs.inorgchem.5b01125
Inorg. Chem. 2015, 54, 7968−7975

Table 1. Reaction Parameters and Final Product Phase from Route 3

	OAm	TOP	OAm/TOP	TOP/Ni	product phase
a	1.0 mmol	22.4 mmol	0.045	33.4	NiP_2
b	15.0 mmol	22.4 mmol	0.67	33.4	NiP_2, Ni_5P_4
c	30.0 mmol	22.4 mmol	1.34	33.4	Ni_5P_4
d	30.0 mmol	3.36 mmol	8.93	5.01	Ni_5P_4, Ni_2P
e	30.0 mmol	2.24 mmol	13.39	3.34	Ni_2P

CONCLUSIONS

The various roles of reaction parameters on the extent of phosphidation of Ni to produce crystalline nanoparticles of Ni_2P, Ni_5P_4, or NiP_2 from the reaction of nickel complexes with TOP in OAm solutions are depicted in Scheme 2. With or without the 230 °C intermediate step, for a constant concentration of Ni precursor in the system, increasing the TOP/OAm ratio, reaction temperature, and time favors the formation of more P-rich phases. However, the use of an intermediate 230 °C soak step, common to metal phosphide nanoparticle syntheses, was found to have no effect on the synthesis of Ni_2P nanoparticles but dramatically reduced the extent of phosphidation possible, even at very high TOP/Ni ratios, producing Ni_5P_4 or NiP_2 samples that always had significant Ni_2P impurities. Particles of Ni_5P_4 and NiP_2 could be obtained as phase-pure products when the intermediate 230 °C step was removed. The OAm/TOP ratio also has a strong effect on the system, enabling tuning from pure Ni_2P to Ni_5P_4 and NiP_2 by decreasing the OAm/TOP ratio. Additionally, large concentrations of OAm attenuate the behavior of different Ni reagents (COD, acac, or OAc complexes), likely by formation of a common intermediate, leading preferentially to Ni_5P_4 unless the TOP/Ni ratio is dramatically reduced, favoring Ni_2P. At a low OAm/TOP ratio, the chelate complex $Ni(acac)_2$ favors Ni_5P_4 (i.e., less Ni available in the reaction) and $Ni(OAc)_2$ favors Ni_2P. Under the extreme phosphidation conditions required to favor Ni_5P_4 and NiP_2 (large excess of TOP), the 20−30 nm crystallites assemble into supraparticles with diameters of 100−500 nm. Overall, this work addresses a knowledge gap in the phase evolution for the P rich side of the Ni−P nanoparticle system. The strategy used to prepare more P-rich nickel phosphide nanoparticles should be applicable to other metal phosphide systems, thus facilitating the development of this important class of nanomaterials for energy storage and catalysis.

ASSOCIATED CONTENT

Supporting Information

The Supporting Information is available free of charge on the ACS Publications website at DOI: 10.1021/acs.inorgchem.5b01125.

PXRD patterns and TEM images of Ni_2P prepared with and without the intermediate heating step; PXRD patterns of nickel phosphides prepared by route 3 as a function of heating temperature, time and P/Ni ratio (figures) (PDF)

AUTHOR INFORMATION

Corresponding Author

*E-mail: sbrock@chem.wayne.edu.

Present Address

†Department of Chemistry, Florida A&M University, Tallahassee, FL 32307

Author Contributions

Early work was performed by Lance Aquilina and Keerthi Senevirathne to identify that Ni_5P_4 could be synthesized by standard arrested precipitation routes, and both of these coauthors provided comments on the final version of the paper. D.L. optimized synthesis of Ni_5P_4 and NiP_2, elucidated the roles of factors in the synthesis, and drafted the manuscript.

Scheme 2. Illustration of the Roles Played by Various Synthetic Levers in Controlling the Phase in Nickel Phosphide Nanoparticles[a]

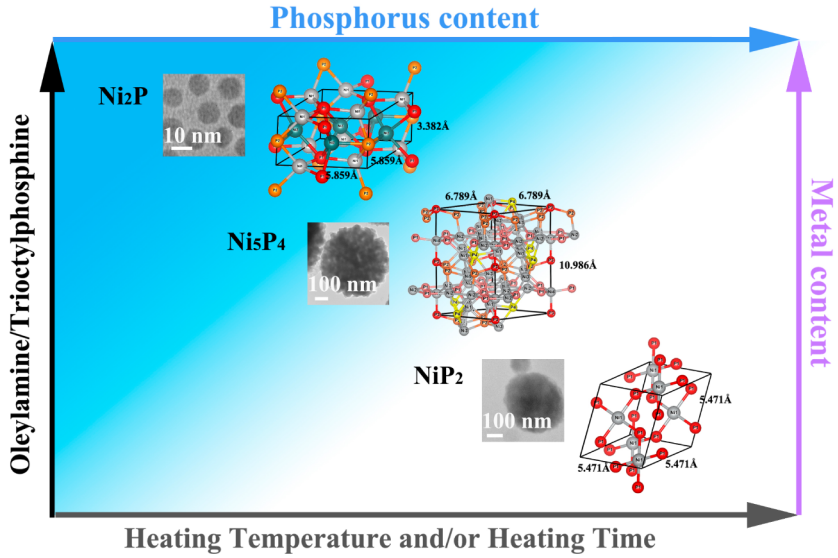

[a]The crystal structures shown inside correspond to Ni_2P (hexaganol), Ni_5P_4 (hexaganol), and NiP_2 (cubic) and were drawn with the software VESTA 3.[30]

DOI: 10.1021/acs.inorgchem.5b01125
Inorg. Chem. 2015, 54, 7968−7975

Funding

This work was performed with financial support from NSF-DMR (1361470) and Wayne State University (Rumble Fellowship to D.L.).

Notes

The authors declare no competing financial interest.

■ ACKNOWLEDGMENTS

We acknowledge financial support from NSF-DMR (1361470) and Wayne State University (Rumble Fellowship to D.L.). We thank Z. Mei and R. Baird for assistance with electron microscopy and powder X-ray diffraction, respectively. TEM and powder X-ray powder diffraction data were acquired at the Lumigen Instrument Center, Wayne State University

■ REFERENCES

(1) Brock, S. L.; Perera, S. C.; Stamm, K. L. *Chem. - Eur. J.* **2004**, *10*, 3364−3371.
(2) Brock, S. L.; Senevirathne, K. *J. Solid State Chem.* **2008**, *181*, 1552−1559.
(3) Oyama, S. T. *J. Catal.* **2003**, *216*, 343−352.
(4) Popczun, E. J.; Read, C. G.; Roske, C. W.; Lewis, N. S.; Schaak, R. E. *Angew. Chem., Int. Ed.* **2014**, *53*, 5427−5430.
(5) Layan Savithra, G. H.; Muthuswamy, E.; Bowker, R. H.; Carrillo, B. A.; Bussell, M. E.; Brock, S. L. *Chem. Mater.* **2013**, *25*, 825−833.
(6) Muthuswamy, E.; Kharel, P. R.; Lawes, G.; Brock, S. L. *ACS Nano* **2009**, *3*, 2383−2393.
(7) Gaudette, A. F.; Burns, A. W.; Hayes, J. R.; Smith, M. C.; Bowker, R. H.; Seda, T.; Bussell, M. E. *J. Catal.* **2010**, *272*, 18−27.
(8) Senevirathne, K.; Burns, A. W.; Bussell, M. E.; Brock, S. L. *Adv. Funct. Mater.* **2007**, *17*, 3933−3939.
(9) Ha, D. H.; Moreau, L. M.; Bealing, C. R.; Zhang, H. T.; Hennig, R. G.; Robinson, R. D. *J. Mater. Chem.* **2011**, *21*, 11498−11510.
(10) Badari, C. A.; Lonyi, F.; Drotar, E.; Kaszonyi, A.; Valyon, J. *Appl. Catal., B* **2015**, *164*, 48−60.
(11) Sawhill, S. J.; Layman, K. A.; Van Wyk, D. R.; Engelhard, M. H.; Wang, C.; Bussell, M. E. *J. Catal.* **2005**, *231*, 300−313.
(12) Wang, J. L.; Yang, Q.; Zhang, Z. D.; Sun, S. H. *Chem. - Eur. J.* **2010**, *16*, 7916−7924.
(13) Ma, J. J.; Ni, S. B.; Lv, X. H.; Yang, X. L.; Zhang, L. L. *Mater. Lett.* **2014**, *133*, 94−96.
(14) Aso, K.; Hayashi, A.; Tatsumisago, M. *Inorg. Chem.* **2011**, *50*, 10820−10824.
(15) Laursen, A. B.; Patraju, K. R.; Whitaker, M.; Retuerto, M.; Sarkar, T.; Yao, N.; Ramanujachary, K. V.; Greenblatt, M.; Dismukes, G. C. *Energy Environ. Sci.* **2015**, *8*, 1027−1034.
(16) Jiang, P.; Liu, Q.; Sun, X. P. *Nanoscale* **2014**, *6*, 13440−13445.
(17) Popczun, E. J.; McKone, J. R.; Read, C. G.; Biacchi, A. J.; Wiltrout, A. M.; Lewis, N. S.; Schaak, R. E. *J. Am. Chem. Soc.* **2013**, *135*, 9267−9270.
(18) Henkes, A. E.; Schaak, R. E. *Chem. Mater.* **2007**, *19*, 4234−4242.
(19) Muthuswamy, E.; Savithra, G. H. L.; Brock, S. L. *ACS Nano* **2011**, *5*, 2402−2411.
(20) Barry, B. M.; Gillan, E. G. *Chem. Mater.* **2008**, *20*, 2618−2620.
(21) Carenco, S.; Boissiere, C.; Nicole, L.; Sanchez, C.; Le Floch, P.; Mezailles, N. *Chem. Mater.* **2010**, *22*, 1340−1349.
(22) Moreau, L. M.; Ha, D.-H.; Bealing, C. R.; Zhang, H.; Hennig, R. G.; Robinson, R. D. *Nano Lett.* **2012**, *12*, 4530−4539.
(23) Carenco, S.; Hu, Y.; Florea, I.; Ersen, O.; Boissiere, C.; Mezailles, N.; Sanchez, C. *Chem. Mater.* **2012**, *24*, 4134−4145.
(24) Wang, J. W.; Johnston-Peck, A. C.; Tracy, J. B. *Chem. Mater.* **2009**, *21*, 4462−4467.
(25) Moreau, L. M.; Ha, D. H.; Zhang, H. T.; Hoyden, R.; Muller, D. A.; Robinson, R. D. *Chem. Mater.* **2013**, *25*, 2394−2403.
(26) Xia, Y.; Tang, Z. *Chem. Commun.* **2012**, *48*, 6320−6336.
(27) Liu, J.; Sun, Z. K.; Deng, Y. H.; Zou, Y.; Li, C. Y.; Guo, X. H.; Xiong, L. Q.; Gao, Y.; Li, F. Y.; Zhao, D. Y. *Angew. Chem., Int. Ed.* **2009**, *48*, 5875−5879.
(28) Narayanaswamy, A.; Xu, H.; Pradhan, N.; Peng, X. *Angew. Chem., Int. Ed.* **2006**, *45*, 5361−5364.
(29) Xia, Y.; Nguyen, T. D.; Yang, M.; Lee, B.; Santos, A.; Podsiadlo, P.; Tang, Z.; Glotzer, S. C.; Kotov, N. A. *Nat. Nanotechnol.* **2011**, *6*, 580−587.
(30) Momma, K.; Izumi, F. *J. Appl. Crystallogr.* **2011**, *44*, 1272−1276.

DOI: 10.1021/acs.inorgchem.5b01125
Inorg. Chem. 2015, 54, 7968−7975